

Constraints on Non-Standard Neutrino Interactions and Unparticle Physics with $\bar{\nu}_e - e^-$ Scattering at the Kuo-Sheng Nuclear Power Reactor

M. Deniz,^{1,2} S. Bilmiş,^{1,2} İ.O. Yıldırım,^{1,2} H.B. Li,¹ J. Li,^{3,4} H.Y. Liao,¹ C.W. Lin,¹ S.T. Lin,¹ M. Serin,² V. Singh,^{1,6} H.T. Wong,^{1,*} S.C. Wu,¹ Q. Yue,⁴ M. Zeyrek,² and Z.Y. Zhou⁵

(TEXONO Collaboration)

¹ *Institute of Physics, Academia Sinica, Taipei 11529, Taiwan.*

² *Department of Physics, Middle East Technical University, Ankara 06531, Turkey.*

³ *Institute of High Energy Physics, Chinese Academy of Science, Beijing 100039, China.*

⁴ *Department of Engineering Physics, Tsinghua University, Beijing 100084, China.*

⁵ *Department of Nuclear Physics, Institute of Atomic Energy, Beijing 102413, China.*

⁶ *Department of Physics, Banaras Hindu University, Varanasi 221005, India.*

(Dated: November 1, 2018)

Neutrino-electron scatterings are purely leptonic processes with robust Standard Model (SM) predictions. Their measurements can therefore provide constraints to physics beyond SM. The $\bar{\nu}_e - e$ data taken at the Kuo-Sheng Reactor Neutrino Laboratory were used to probe two scenarios: Non-Standard Neutrino Interactions (NSI) and Unparticle Physics. New constraints were placed to the NSI parameters $(\varepsilon_{ee}^{eL}, \varepsilon_{ee}^{eR})$, $(\varepsilon_{e\mu}^{eL}, \varepsilon_{e\mu}^{eR})$ and $(\varepsilon_{e\tau}^{eL}, \varepsilon_{e\tau}^{eR})$ for the Non-Universal and Flavor-Changing channels, respectively, as well as to the coupling constants for scalar (λ_0) and vector (λ_1) unparticles to the neutrinos and electrons.

PACS numbers: 13.15.+g, 14.60.St, 25.30.Pt

I. INTRODUCTION

The compelling evidence of neutrino oscillations from the solar, atmospheric as well as long baseline accelerator and reactor neutrino measurements implies finite neutrino masses and mixings [1]. Their physical origin and experimental consequences have not been fully understood yet. Experimental studies on the neutrino properties and interactions are crucial because they can shed light to these fundamental questions and may provide hints or constraints to models on new physics. Reactor neutrino is an excellent neutrino source to address many of the issues, because of its high flux and availability. The reactor $\bar{\nu}_e$ spectra is understood and known, while reactor ON/OFF comparison provides model-independent means of background subtraction.

Neutrino-electron scatterings are purely leptonic processes with robust Standard Model (SM) predictions [2]. Experiments on $\nu_e(\bar{\nu}_e)$ scattering [3] have played important roles in testing SM, and in the studies of neutrino intrinsic properties and oscillation. We report in this paper experimental constraints on neutrino non-standard interactions (NSI) and on neutrino unparticle physics (UP) couplings derived from published results [4–6] from $\bar{\nu}_e - e$ scattering experiments at the Kuo-Sheng Nuclear Power Station in Taiwan.

II. ELECTRON ANTINEUTRINO-ELECTRON SCATTERING

A. Standard Model

The SM cross-section at the laboratory frame $\nu_\mu(\bar{\nu}_\mu) - e$ elastic scattering, where only neutral-current is involved, is given by [2, 3]:

$$\left[\frac{d\sigma}{dT}(\bar{\nu}_\mu e) \right]_{SM} = \frac{G_F^2 m_e}{2\pi} \cdot [(g_V \pm g_A)^2 + (g_V \mp g_A)^2 \left(1 - \frac{T}{E_\nu} \right)^2 - (g_V^2 - g_A^2) \frac{m_e T}{E_\nu^2}] \quad (1)$$

where G_F is the Fermi coupling constant, T is the kinetic energy of the recoil electron, E_ν is the incident neutrino energy and g_V, g_A are the vector and axial-vector coupling constants, respectively. The upper(lower) sign refers to the interactions with $\nu_\mu(\bar{\nu}_\mu)$. The SM assignments to the coupling constants are: $g_V = -\frac{1}{2} + 2\sin^2\theta_W$ and $g_A = -\frac{1}{2}$, where $\sin^2\theta_W$ is the weak mixing angle.

The $\nu_e(\bar{\nu}_e) - e$ interaction is among the few SM processes which proceed via *both* charged- and neutral-currents, in addition to their interference effects [7]. The cross-section can be obtained by making the replacement of $g_{V,A} \rightarrow (g_{V,A} + 1)$ in Eq. 1. In the case of $\bar{\nu}_e - e$ which

*Corresponding Author: htwong@phys.sinica.edu.tw; Tel:+886-2-2789-9682; FAX:+886-2-2788-9828.

is relevant for reactor neutrinos,

$$\left[\frac{d\sigma}{dT}(\bar{\nu}_e e) \right]_{SM} = \frac{G_F^2 m_e}{2\pi} \cdot [(g_V - g_A)^2 + (g_V + g_A + 2)^2 \left(1 - \frac{T}{E_\nu}\right)^2 - (g_V - g_A)(g_V + g_A + 2) \frac{m_e T}{E_\nu^2}] . \quad (2)$$

By defining chiral couplings g_L and g_R :

$$\begin{aligned} g_L &= \frac{1}{2}(g_V + g_A) = -\frac{1}{2} + \sin^2\theta_W \quad \text{and} \\ g_R &= \frac{1}{2}(g_V - g_A) = \sin^2\theta_W \quad , \end{aligned} \quad (3)$$

Eq. 2 can be expressed as

$$\left[\frac{d\sigma}{dT}(\bar{\nu}_e e) \right]_{SM} = \frac{2G_F^2 m_e}{\pi} \cdot [g_R^2 + (g_L + 1)^2 \left(1 - \frac{T}{E_\nu}\right)^2 - g_R(g_L + 1) \frac{m_e T}{E_\nu^2}] . \quad (4)$$

B. Non-Standard Neutrino Interactions

Non-standard interactions (NSI) of neutrinos were introduced in the early work on neutrino matter effects via alternative mechanisms [8]. Models on massive neutrinos generally give rise to NSI. Examples [9] include seesaw type models, low energy SUSY with R-parity breaking, models acquiring mass radiatively due to the presence of extra Higgs boson, unified SUSY models as a renormalization effect. Constraints or evidence of NSI are relevant to the interpretations of sub-leading contributions in the forthcoming precision neutrino oscillation experiments [1, 10], and have consequences in astrophysics [11] such as the understanding of supernova explosion.

Phenomenology of NSI has been explored with a variety of neutrino sources and interaction channels [11–16]. This can be studied with short baseline experiments where the neutrino fluxes are high and the oscillation effects can be neglected. A model independent approach is to incorporate new NSI couplings in the neutrino sector to the SM electroweak parameters, as illustrated schematically in Figure 1a. The NSI of $\bar{\nu}_\alpha - e$ scattering is described by an effective Lagrangian:

$$\mathcal{L}_{\text{eff}} = -\epsilon_{\alpha\beta}^{eP} 2\sqrt{2}G_F(\bar{\nu}_\alpha\gamma_\rho L\nu_\beta)(\bar{e}\gamma^\rho P e) \quad , \quad (5)$$

where $\epsilon_{\alpha\beta}^{eP}$ describes the coupling strength with respect to G_F . The helicity states are denoted by P (=L,R), and (α, β) stand for the lepton flavor (e, μ or τ). The cases where $\alpha = \beta$ and $\alpha \neq \beta$ correspond to Non-Universal (NU) and Flavor-Changing (FC) NSI, respectively.

For reactor neutrinos, $\alpha = e$, and six parameters are involved – the NU $\epsilon_{ee}^{eL,R}$ as well as the FC $\epsilon_{e\mu}^{eL,R}$ and

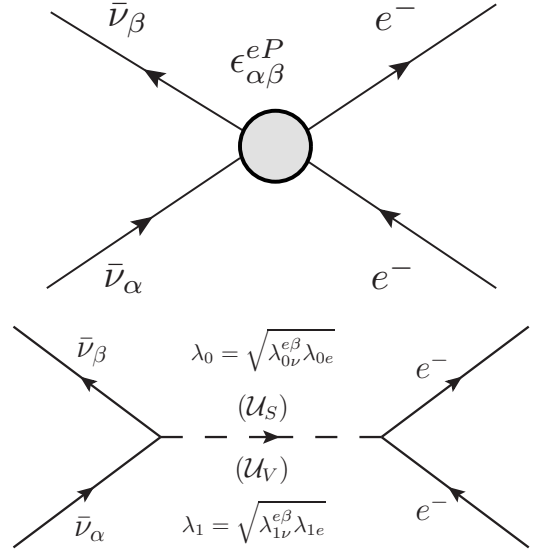


Figure 1: Top: (a) NSI of neutrinos, generically described as four-Fermi interaction with new couplings. Bottom: (b) Interactions of neutrino with electron via exchange of virtual scalar \mathcal{U}_S and vector \mathcal{U}_V unparticle.

$\epsilon_{e\tau}^{eL,R}$. The cross-section formula including both SM and NSI interactions for $\bar{\nu}_e + e \rightarrow \bar{\nu}_e + e$ is given by [13, 14]

$$\left[\frac{d\sigma}{dT} \right]_{SM+NSI} = \frac{2G_F^2 m_e}{\pi} \cdot \left[\tilde{g}_R^2 + \sum_{\alpha \neq e} |\epsilon_{\alpha e}^{eR}|^2 + \left((\tilde{g}_L + 1)^2 + \sum_{\alpha \neq e} |\epsilon_{\alpha e}^{eL}|^2 \right) \left(1 - \frac{T}{E_\nu}\right)^2 - \left(\tilde{g}_R(\tilde{g}_L + 1) + \sum_{\alpha \neq e} |\epsilon_{\alpha e}^{eR}| |\epsilon_{\alpha e}^{eL}| \right) \frac{m_e T}{E_\nu^2} \right] , \quad (6)$$

where $\tilde{g}_L = g_L + \epsilon_{ee}^{eL}$ and $\tilde{g}_R = g_R + \epsilon_{ee}^{eR}$.

The measurable recoil spectra at a typical reactor flux of $\phi(\bar{\nu}_e) = 10^{13} \text{ cm}^{-2}\text{s}^{-1}$ are displayed in Figure 2a, at NSI parameters in both NU and FC channels relevant to this work. The SM spectrum is superimposed. The NSI contributions give rise to similar spectral shapes as the SM one. Accordingly, the appropriate strategy to study NSI is to focus at the MeV energy range where the SM effects were measured with good accuracy [4].

The strong experimental limits on the branching ratio of $\mu \rightarrow 3e$ in accelerator experiments provided stringent bounds on $|\epsilon_{e\mu}^{eL,R}| < 5 \times 10^{-4}$ [13], which is highly sensitive to loop processes. Model independent analysis after taking gauge invariance into account gave rise to weaker bounds on $|\epsilon_{e\mu}^{eL,R}| < 0.1$ [15]. We present results on the FC parameters $\epsilon_{e\mu}^{eL,R}$ and $\epsilon_{e\tau}^{eL,R}$, as well as the NU parameters $\epsilon_{ee}^{eL,R}$ in this analysis with reactor $\bar{\nu}_e$ data.

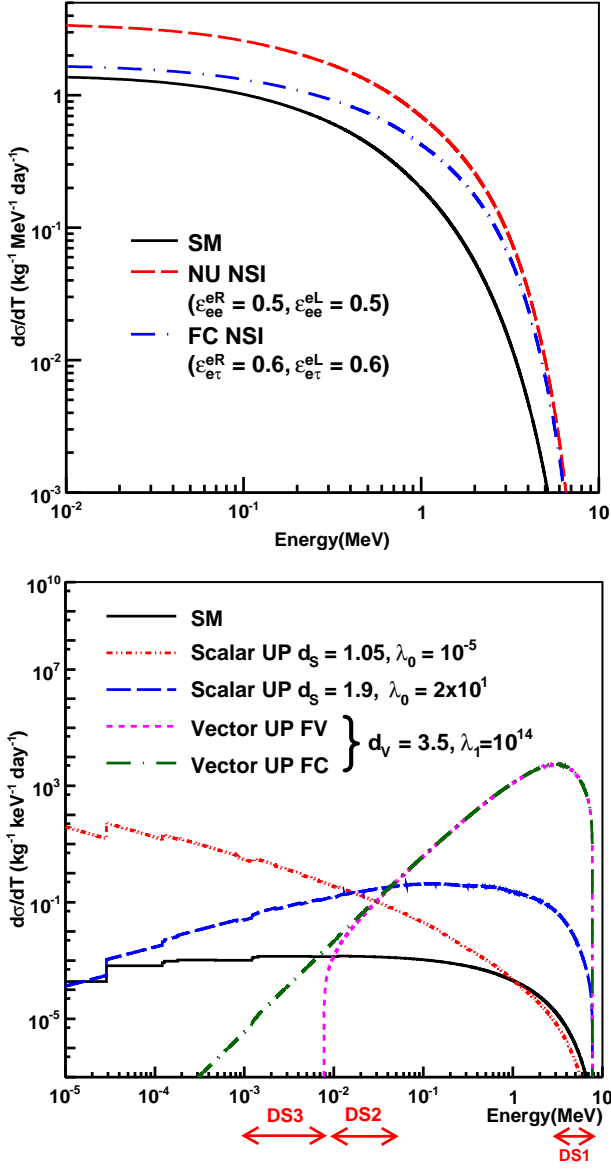


Figure 2: Differential cross-section as function of the recoil energy T with typical reactor- $\bar{\nu}_e$ spectra. Top: (a) NSI at coupling parameters relevant to this work using CsI(Tl) as target. Bottom: (b) scalar UP, at two values of (d_S, λ_0) and vector UP, at a value of (d_V, λ_1) for both FV and FC cases, using Ge as target. The SM contributions are also superimposed. The relevant energy ranges of the three data sets used in the present analysis are also shown.

C. Unparticle Physics

A scale invariant sector can be described by Banks-Zaks (BZ) fields which is related to gauge theories with non-integer number of fermions [17]. BZ fields has its own gauge group and do not couple to the SM fields which have definite masses. It has been proposed [18] that both the SM and BZ fields may coexist in a high energy scale. Below an energy scale Λ_U , BZ operators turn into unpar-

ticle operators \mathcal{O}_U with a non-integer scaling dimension, denoted by d_S and d_V for the scalar and vector cases, respectively.

Unparticle effects can be studied in accelerator experiments [19] through their direct production, the signatures of which are missing energy in the detectors. An alternative method is to probe the virtual effects of unparticles which act as mediators in the interactions [18, 19]. This approach was adopted in the present analysis using reactor neutrinos as probe. The interaction Lagrangians for $\nu_\alpha + e \rightarrow \nu_\beta + e$ via virtual scalar and vector unparticle exchange as depicted in Figure 1b are given, respectively, by [19–22]

$$\mathcal{L}_{J=0} = \frac{\lambda_{0e}}{\Lambda_U^{d_S-1}} \bar{e}e \mathcal{O}_U + \frac{\lambda_{0\nu}^{\alpha\beta}}{\Lambda_U^{d_S-1}} \bar{\nu}_\alpha \nu_\beta \mathcal{O}_U \quad \text{and} \quad (7)$$

$$\mathcal{L}_{J=1} = \frac{\lambda_{1e}}{\Lambda_U^{d_V-1}} \bar{e} \gamma_\mu e \mathcal{O}_U^\mu + \frac{\lambda_{1\nu}^{\alpha\beta}}{\Lambda_U^{d_V-1}} \bar{\nu}_\alpha \gamma_\mu \nu_\beta \mathcal{O}_U^\mu, \quad (8)$$

where λ_{J_e} and $\lambda_{J\nu}^{\alpha\beta}$ are the corresponding coupling constants with $J = 0, 1$ denoting scalar and vector unparticle interactions, respectively.

The cross-section of $\bar{\nu}_e - e$ scattering with scalar unparticle exchange is given by

$$\left(\frac{d\sigma}{dT} \right)_{\mathcal{U}_S} = \frac{f_0^2(d_S)}{\Lambda_U^{4d_S-4}} \frac{2^{2d_S-6}}{\pi E_\nu^2} (m_e T)^{2d_S-3} (T+2m_e), \quad (9)$$

where

$$f_0(d_S) = \frac{\lambda_{0\nu}^{\alpha\beta} \lambda_{0e}}{2 \sin(d_S \pi)} A_0(d_S) \quad (10)$$

and the normalization constant $A_0(d_S)$ is given by:

$$A_0(d_S) = \frac{16\pi^{5/2}}{(2\pi)^{2d_S}} \frac{\Gamma(d_S + 1/2)}{\Gamma(d_S - 1)\Gamma(2d_S)}. \quad (11)$$

The interference effects with SM are negligible due to suppression by factors of m_ν/Λ_U . Therefore, it is not necessary to differentiate flavor conserving (FC) and violating (FV) scalar UP interactions.

The cross-section of $\bar{\nu}_e - e$ scattering via vector UP exchange is

$$\begin{aligned} \left(\frac{d\sigma}{dT} \right)_{\mathcal{U}_V} &= \frac{1}{\pi} \frac{f_1^2(d_V)}{\Lambda_U^{4d_V-4}} 2^{2d_V-5} m_e^{2d_V-3} T^{2d_V-4} \\ &\times \left[1 + \left(1 - \frac{T}{E_\nu} \right)^2 - \frac{m_e T}{E_\nu^2} \right], \quad (12) \end{aligned}$$

where $f_1(d_V)$ follows a similar expression as Eq. 10, making the replacement $\lambda_{0\nu}^{\alpha\beta} \lambda_{0e} \rightarrow \lambda_{1\nu}^{\alpha\beta} \lambda_{1e}$ and $A_0(d_S) \rightarrow A_1(d_V)$. Unlike the scalar UP case, the interference effects with SM also contribute in the vector UP interac-

tions:

$$\begin{aligned} \left(\frac{d\sigma}{dT}\right)_{\nu-SM} &= \frac{\sqrt{2}G_F}{\pi} \frac{f_1(d_\nu)}{\Lambda_U^{2d_\nu-2}} (2m_e T)^{d_\nu-2} m_e \\ &\times [g_R + (g_L + 1) \left(1 - \frac{T}{E_\nu}\right)^2 \\ &- \frac{(g_L + g_R + 1)m_e T}{2E_\nu^2}]. \end{aligned} \quad (13)$$

The FV and FC cross-sections for vector UP are therefore given by Eq. 12 and the sum of Eq. 12 and Eq. 13, respectively.

The differential cross-sections of the UP interactions using Ge as target are displayed in Figure 2b with the SM contributions superimposed for comparison. The sawtooth structures for $T \lesssim 1$ keV are due to suppression by the atomic binding energy [23].

Three sets of parameters characterize the unparticle interactions and can be probed experimentally: (i) unparticle energy scale Λ_U , (ii) unparticle mass dimensions d_S and d_V , as well as (ii) coupling constants $\lambda_0 \equiv \sqrt{\lambda_{0\nu}^{e\beta}\lambda_{0e}}$ and $\lambda_1 \equiv \sqrt{\lambda_{1\nu}^{e\beta}\lambda_{1e}}$ for the scalar and vector UP interactions, respectively. The UP energy scale is taken to be $\Lambda_U \sim 1$ TeV in most recent work [21, 22, 24]. Unitarity requirement placed constraints on the dimension [25] to be within $1 < d_S < 2$ in the scalar case, but only provides lower bound $d_V \geq 3$ for vector UP exchange. The spectral shape of Figure 2b and the T -dependence of Eq. 9 indicate that measurements with low energy threshold are expected to provide better sensitivities at $d_S < 3/2$. On the other hand, high energy experiments are preferred to probe UP due to the large values of d_S and d_V .

III. EXPERIMENTAL CONSTRAINTS

A. Merits of Reactor Neutrinos

Several features make short-baseline reactor neutrino experiments optimal for probing physics beyond SM [12]. Reactor neutrinos are pure $\bar{\nu}_e$ which simplifies interpretations of the results. Atmospheric and solar neutrinos have different eigenstate compositions at the detectors. The constraints from these experiments therefore are not identical to those at reactors, analogous to the studies of neutrino magnetic moments [26].

Experimentally reactors produce high $\bar{\nu}_e$ -fluxes compared to other sources. The reactor OFF periods provide model-independent means of background subtraction. It was recently recognized [4] that the studies of reactor $\bar{\nu}_e - e$ provide better sensitivities to the SM electroweak parameters $\sin^2\theta_W$ and (g_V, g_A) at the same experimental accuracies as those from $\nu_e - e$ measurements. The lower neutrino energy at the MeV range also favors applications where sensitivities can be enhanced at low detector threshold.

B. Input Data

Data adopted for this analysis were taken at the Kuo Sheng Neutrino Laboratory (KSNL) located at a distance of 28 m from the reactor core. The nominal thermal power output was 2.9 GW producing an average $\bar{\nu}_e$ -flux of $\phi(\bar{\nu}_e) \sim 6.4 \times 10^{12} \text{ cm}^{-2}\text{s}^{-1}$ [5]. Detectors were placed inside a shielding structure where ambient radioactivity was suppressed by 50 tons of passive materials.

Three independent data sets were adopted, each having a different energy range as depicted in Figure 2.

DS1-CsI(Tl): Data with 29882/7369 kg-days of Reactor ON/OFF exposure of a CsI(Tl) crystal scintillator array [4] with a total mass of 187 kg. Analysis range is 3 – 8 MeV. From the excess of events in the ON–OFF residual spectrum, the SM electroweak angle was measured to be $\sin^2\theta_W = 0.251 \pm 0.031(stat) \pm 0.024(sys)$ which improved over previous results from $\bar{\nu}_e - e$ scattering and was comparable to those from $\nu_e - e$ experiments.

DS2-HPGe: Data with 570.7/127.8 kg-days of Reactor ON/OFF exposure taken with a high-purity germanium (HPGe) detector [5] with a target mass of 1.06 kg. Analysis threshold of 10 keV with a background level of $\sim 1 \text{ kg}^{-1}\text{keV}^{-1}\text{day}^{-1}$ was achieved. The low threshold allowed sensitive limits on neutrino magnetic moments to be derived from the ON–OFF residual spectrum.

DS3-ULEGe: Data with 0.338 kg-days of Reactor ON exposure taken with an ultra-low-energy germanium (ULEGe) detector array [6] with a total mass of 20 g and a threshold of 220 ± 10 eV. The sub-keV threshold opened a window of studying WIMP dark matter with mass less than 10 GeV.

The three data sets (DS1–3) are displayed in Figures 3a,b&c, respectively. Their respective energy ranges are depicted in Figure 2. The SM contributions from $\bar{\nu}_e - e$ are superimposed in (a) and (b), and are out of range at $\sim 10^{-3} \text{ kg}^{-1}\text{keV}^{-1}\text{day}^{-1}$ in (c). The NSI or UP scenarios where the data sets would be optimal to provide sensitive bounds were selected. The observable spectra of an excluded and an allowed parameter space were superimposed as illustrations.

The observed event rates (R_{expt}) of the various data sets, in units of $\text{kg}^{-1}\text{keV}^{-1}\text{day}^{-1}$, were compared to the expected rates (R_X) evaluated for the different interaction channels X ($X = SM, NSI, UP$), via

$$R_X = \rho_e \int_T \int_{E_\nu} \left(\frac{d\sigma}{dT}\right)_X \frac{d\phi(\bar{\nu}_e)}{dE_\nu} dE_\nu dT, \quad (14)$$

where ρ_e is the electron number density per kg of target mass, and $d\phi(\bar{\nu}_e)/dE_\nu$ corresponds to the neutrino spectrum. Constraints were then derived.

Different analysis algorithms were necessary for the three data sets. A minimum- χ^2 fit was performed for

Table I: Constraints at 90% CL due to one-parameter fits on the NSI couplings. The results are presented as “best-fit \pm statistical error \pm systematic error”. Bounds from LSND [13] and combined data [14], as well as from a model-independent analysis [15] are compared with those of this work. The projected statistical sensitivities correspond to a potential measurement of the SM cross-section at 2% accuracy [4].

NSI		TEXONO (This Work)			LSND [13]	Combined [14]	Ref. [15]	
Parameters	Measurement	χ^2/dof	Bounds at 90% CL	Projected Sensitivities	Bounds at 90% CL			
NU {	ε_{ee}^{eL}	$\varepsilon_{ee}^{eL} =$	8.9/9	$-1.53 < \varepsilon_{ee}^{eL} < 0.38$	± 0.015	$-0.07 < \varepsilon_{ee}^{eL} < 0.11$	$-0.03 < \varepsilon_{ee}^{eL} < 0.08$	$ \varepsilon_{ee}^{eL} < 0.06$
	ε_{ee}^{eR}	$\varepsilon_{ee}^{eR} =$	8.7/9	$-0.07 < \varepsilon_{ee}^{eR} < 0.08$	± 0.002	$-1.0 < \varepsilon_{ee}^{eR} < 0.5$	$0.004 < \varepsilon_{ee}^{eR} < 0.151$	$ \varepsilon_{ee}^{eR} < 0.14$
		$0.02 \pm 0.04 \pm 0.02$						
FC {	$\varepsilon_{e\mu}^{eL}$	$\varepsilon_{e\mu}^{eL^2}(\varepsilon_{e\tau}^{eL^2}) =$	8.9/9	$ \varepsilon_{e\mu}^{eL} < 0.84$	± 0.052	—	$ \varepsilon_{e\mu}^{eL} < 0.13$	$ \varepsilon_{e\mu}^{eL} < 0.1$
	$\varepsilon_{e\tau}^{eL}$							
	$\varepsilon_{e\mu}^{eR}$	$\varepsilon_{e\mu}^{eR^2}(\varepsilon_{e\tau}^{eR^2}) =$	8.7/9	$ \varepsilon_{e\mu}^{eR} < 0.19$	± 0.007	—	$ \varepsilon_{e\mu}^{eR} < 0.13$	$ \varepsilon_{e\mu}^{eR} < 0.1$
	$\varepsilon_{e\tau}^{eR}$							

DS1-CsI(Tl) and DS2-HPGe, with

$$\chi^2 = \sum_{i=1} \left[\frac{R_{\text{expt}}(i) - [R_{SM}(i) + R_X(i)]}{\Delta_{\text{stat}}(i)} \right]^2, \quad (15)$$

where $R_{SM}(i)$ and $R_X(i)$ are the expected event rates on the i^{th} data bin due to the SM and X(=NSI or UP) contributions, respectively, while $\Delta_{\text{stat}}(i)$ is the corresponding uncertainty of the measurement. For DS3-ULEGe, there was no corresponding Reactor OFF data so that the conventional Reactor ON–OFF background subtraction and a best-fit analysis were not possible. Instead, the “Binned Poisson” method developed for dark matter searches [27] was adopted. No background assumption was made such that upper bounds on NSI or UP-induced contributions were placed since they could not be larger than the observed signals.

C. Non-Standard Neutrino Interaction

The NSI parameters are constrained by the accuracy of the SM cross-section measurements. Accordingly, DS1-CsI(Tl) was adopted for analysis. The NSI parameters of Eq. 6 were the fitting variables in the minimum- χ^2 analysis.

Results from one-dimensional analysis are presented in Table I. It can be inferred from Eq. 6 that the sensitivities for NU and FC couplings vary as $\varepsilon_{ee}^{eL,R}$ and $[\varepsilon_{e\mu}^{eL,R}]^2([\varepsilon_{e\tau}^{eL,R}]^2)$, respectively. New limits on $\varepsilon_{ee}^{eL,R}$, $\varepsilon_{e\mu}^{eL,R}$ and $\varepsilon_{e\tau}^{eL,R}$ were derived. The results on $\varepsilon_{e\mu}^{eL,R}$ and $\varepsilon_{e\tau}^{eL,R}$ are identical since their roles are symmetrical such that one-dimensional analysis cannot differentiate their effects. The projected sensitivities due to a realistically achievable 2% measurement of the SM $\bar{\nu}_e$ –e cross-section with reactor neutrinos [4] are shown. As comparison, we also list the constraints from LSND ν_e –e measurement [13] and those from a combined analysis with data from LEP, CHARM, LSND, and previous reactor experiments [14], as well as a model-independent analysis on $\varepsilon_{e\mu}^{eL,R}$.

The allowed region at 90% confidence level (CL) from two-parameter analysis were displayed in Figures 4a&b in the $(\varepsilon_{ee}^{eL}, \varepsilon_{ee}^{eR})$ and $(\varepsilon_{e\tau}^{eL}, \varepsilon_{e\tau}^{eR})$ space, respectively, in which the bounds from LSND [13] were overlaid. The complementarity between the constraints due to $\bar{\nu}_e$ –e and ν_e –e scatterings can be readily seen. The constraints in the $(\varepsilon_{e\mu}^{eL}, \varepsilon_{e\mu}^{eR})$ plane are the same as those of $(\varepsilon_{e\tau}^{eL}, \varepsilon_{e\tau}^{eR})$ in Figure 4b.

As comparison and for completeness, we also note the bounds on NSI NU and FC couplings in the quark sector due to accelerator νN scattering experiments are $|\epsilon_{ee}^{qP}| < 0.3 - 1$ and $|\epsilon_{e\tau}^{qP}| < 0.5 - 1.6$, respectively [13], where P denotes the helicity-state R/L while $q=u$ or d quarks. Projected sensitivities due to future experiments on neutrino-nucleus coherent scatterings [28] are $|\epsilon_{ee}^{qL} + \epsilon_{ee}^{qR}| < 0.001$ and $|\epsilon_{e\tau}^{qL} + \epsilon_{e\tau}^{qR}| < 0.02$ [16].

D. Unparticle Physics Parameters

Since different ranges of the $d_S(d_\nu)$ give different sensitivities to the cross-section, all three data set were used in the UP analysis for their complementarity. The threshold value of DS2-HPGe was previously used to probe UP phenomenology in Ref. [21]. A different cross-section formula was used and discussed in a later work [22].

Constraints on λ_0 at different d_S for scalar UP exchange was derived at $\Lambda_U = 1$ TeV. The results are shown in Figure 5a, with bounds from the Borexino [24] and MUNU [22] experiments superimposed. The upper bounds for λ_0 at different energy scale Λ_U are shown in Figure 5b. The data of DS2-HPGe provided better sensitivities at $d_S < 1.3$, while DS1-CsI(Tl) gave rise to more stringent limits at larger d_S .

Constraints on vector UP couplings λ_1 as function of d_ν are displayed in Figure 6a. Both FC and FV couplings give similar bounds in this parameter space. The variations of λ_1 for the two cases are depicted in Figures 6b&c as function of the energy scale Λ_U . The DS1-CsI(Tl) data set consistently provided more severe constraints for vec-

tor UP exchanges, since the couplings were enhanced at high energy as indicated in Figure 2b.

Since $(d\sigma/dT)_{\mathcal{U}_S} \propto \lambda_0^4$ and $(d\sigma/dT)_{\mathcal{U}_V} \propto \lambda_1^4$ from Eqs. 9&12, respectively, the potentials on placing more severe constraints on the coupling constants due to improved experimental sensitivities are only modest. When DS1-CsI(Tl) data would improve to provide a 2% measurement of the SM cross-section, an improvement by a factor of 2 to the sensitivities of λ_0 and λ_1 can be expected. Similarly, the benchmark goals of sub-keV ULEGe detectors for studying neutrino-nucleus coherent scattering with reactor neutrinos are to achieve a background level of $\sim 1 \text{ kg}^{-1}\text{keV}^{-1}\text{day}^{-1}$ and ON-OFF sub-

traction of 1% [28]. If these are achieved, the sensitivities of λ_0 and λ_1 would enhance by factor of 2 at $d_S < 1.3$.

IV. ACKNOWLEDGMENTS

The authors appreciate discussions and comments from A. B. Balantekin, M. Blennow, K. Cheung, S. Petcov, T. Rashba and T. C. Yuan. This work is supported by contract 98-9628-M-001-013 under the National Science Council, Taiwan, and by contract 108T502 under TUBITAK, Turkey.

-
- [1] B. Kayser, Phys. Lett. **B 667**, 163 (2008), and references therein.
- [2] J. Erler and P. Langacker, Phys. Lett. **B 667**, 125 (2008), and references therein.
- [3] J. Panman, in *Precision tests of the standard electroweak model*, ed. P. Langacker, 504-544, World Scientific (1995); W. J. Marciano and Z. Parsa, J. Phys. **G 29**, 2629 (2003).
- [4] M. Deniz et al., Phys. Rev. **D 81**, 072001 (2010).
- [5] H. B. Li et al., Phys. Rev. Lett. **90**, 131802 (2003); H. T. Wong et al., Phys. Rev. **D 75**, 012001 (2007).
- [6] S. T. Lin et al., Phys. Rev. **D 79**, 061101(R) (2009).
- [7] B. Kayser et al., Phys. Rev. **D 20**, 87 (1979).
- [8] L. Wolfenstein, Phys. Rev. **D 17**, 2369 (1978); J.W.F. Valle, Phys. Lett. **B 199**, 432 (1987); E. Roulet, Phys. Rev. **D 44**, 935 (1991); M.M. Guzzo, A. Masiero and S.T. Petcov, Phys. Lett. **B 260**, 154 (1991).
- [9] J. Schechter and J. W. F. Valle, Phys. Rev. **D 22**, 2227 (1980); A. Zee, Phys. Lett. **B 93**, 389 (1980); L. J. Hall, V. A. Kostelecky and S. Raby, Nuclear Physics **B 267**, 415 (1986); K. S. Babu, Phys. Lett. **B 203**, 132 (1988); M. Hirsch and J. W. F. Valle, New J. Phys. **6**, 76 (2004).
- [10] Y. Grossman, Phys. Lett. **B 359**, 141 (1995); M. M. Guzzo, P. C. de Holanda and O. L. G. Peres, Phys. Lett. **B 591**, 1 (2004).
- [11] N. Fornengo et al., Phys. Rev. **D 65**, 013010 (2001); P. S. Amanik, G. M. Fuller and B. Grinstein, Astropart. Phys. **24**, 160 (2005); G. L. Fogli, E. Lisi, A. Mirizzi and D. Montanino, Phys. Rev. **D 66**, 013009 (2002); A. Esteban-Pretel, R. Tomas and J. W. F. Valle, Phys. Rev. **D 76**, 053001 (2007).
- [12] O. G. Miranda, M. Maya and R. Huerta, Phys. Rev. **D 53**, 1719 (1996); O. G. Miranda, V. Semikoz and J. W. F. Valle, Nucl. Phys. Proc. Suppl. **66**, 261 (1998); J. Barranco, O. G. Miranda and T. I. Rashba, Phys. Rev. **D 76**, 073008 (2007); A. Bolanos et al., Phys. Rev. **D 79**, 113012 (2009).
- [13] S. Davidson et al., JHEP **0303**, 011 (2003).
- [14] J. Barranco et al., Phys. Rev. **D 73**, 113001 (2006); J. Barranco et al., Phys. Rev. **D 77**, 093014 (2008).
- [15] C. Biggio, M. Blennow and E. Fernandez-Martinez, JHEP **0903**, 139 (2009); C. Biggio, M. Blennow and E. Fernandez-Martinez, JHEP **0908**, 090 (2009).
- [16] J. Barranco, O. G. Miranda and T. I. Rashba, JHEP **0512**, 021 (2005); K. Scholberg, Phys. Rev. **D 73**, 033005 (2006).
- [17] T. Banks and A. Zaks, Nucl. Phys. **B 196**, 189 (1982).
- [18] H. Georgi, Phys. Rev. Lett. **98**, 221601 (2007); H. Georgi, Phys. Lett. **B 650**, 275 (2007).
- [19] K. Cheung, W.Y. Keung and T.C. Yuan, Phys. Rev. Lett. **99**, 051803 (2007); K. Cheung, W.Y. Keung and T.C. Yuan, Phys. Rev. **D 76**, 055003 (2007).
- [20] S. L. Chen and X. G. He, Phys. Rev. **D 76**, 091702 (2007).
- [21] A. B. Balantekin and K. O. Ozansoy, Phys. Rev. **D 76**, 095014 (2007).
- [22] J. Barranco et al., Phys. Rev. **D 79**, 073011 (2009).
- [23] S.A. Fayans, L.A. Mikaelyan and V.V. Sinev, Phys. Atom. Nucl. **64**, 1475 (2001); H.T. Wong, H.B. Li and S.T. Lin, Phys. Rev. Lett., **105**, 061801 (2010).
- [24] D. Montanino, M. Picariello and J. Pulido, Phys. Rev. **D 77**, 093011 (2008).
- [25] S. Zhou, Phys. Lett. **B 659**, 336 (2008); B. Grinstein, K. A. Intriligator and I. Z. Rothstein, Phys. Lett. **B 662**, 367 (2008).
- [26] J.F. Beacom and P. Vogel, Phys. Rev. Lett. **83**, 5222 (1999).
- [27] C. Savage et al., JCAP **04**, 010, Section 3.2 (2009).
- [28] H.T. Wong et al, J. Phys. Conf. Ser. **39**, 266 (2006).

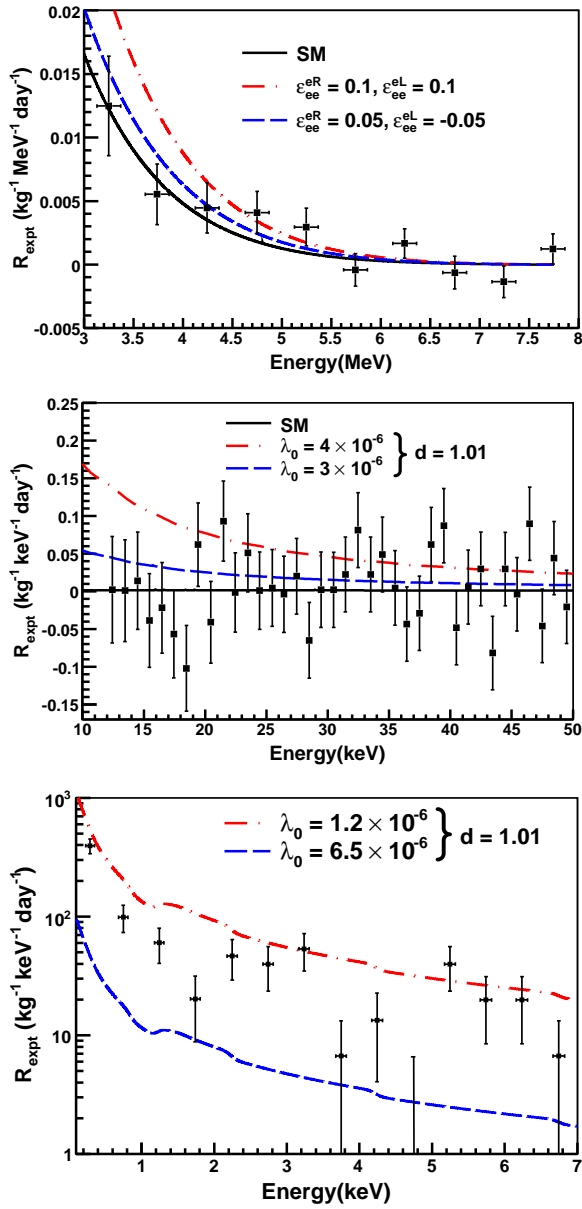


Figure 3: The three data sets adopted for this analysis. Observable NSI or UP spectra at allowed and excluded parameter space are superimposed. Top: (a) DS1-CsI(Tl) Reactor ON-OFF [5], showing SM+NSI with NSI at $(\epsilon_{ee}^R, \epsilon_{ee}^L) = (0.1, 0.1)$ and $(0.05, -0.05)$. Middle: (b) DS2-HPGe Reactor ON-OFF [4], showing SM+UP with $\lambda_0 = 4 \times 10^{-6}$ versus 3×10^{-6} at $d_S = 1.01$. Bottom: (c) DS3-ULEGe Reactor ON only [6], showing SM+UP with $\lambda_0 = 1.2 \times 10^{-5}$ versus 6.5×10^{-6} at $d_S = 1.01$. The SM contributions from $\bar{\nu}_e$ -e are displayed in (a) and (b) as comparison, and are out of range at $\sim 10^{-3} \text{ kg}^{-1} \text{keV}^{-1} \text{day}^{-1}$ in (c).

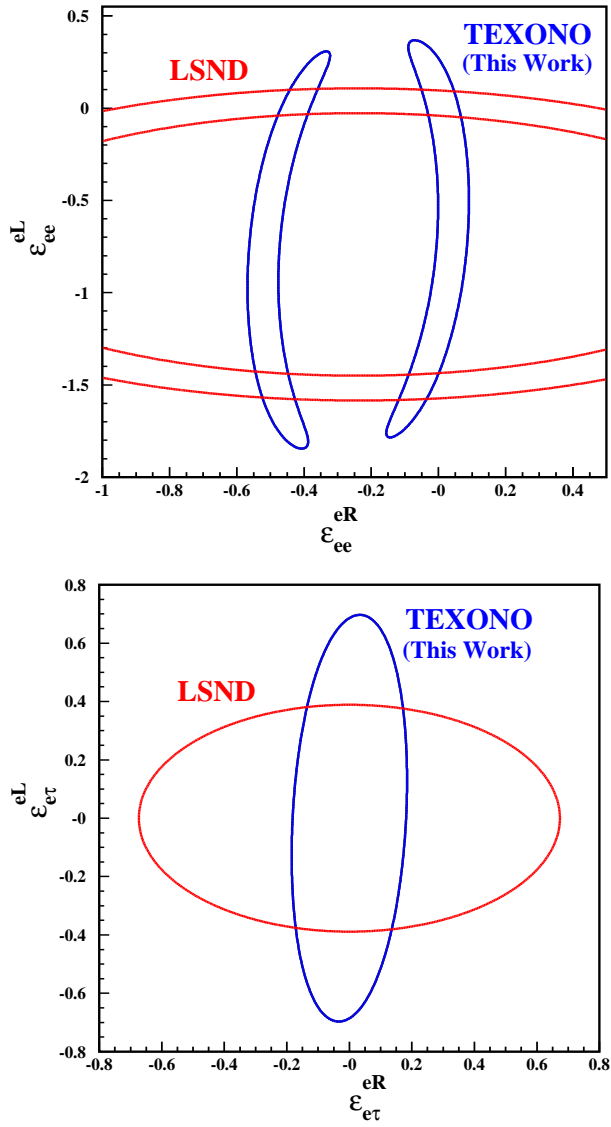


Figure 4: The allowed region at 90% CL for Top: (a) NU NSI parameters of ε_{ee}^{eL} and ε_{ee}^{eR} ; Bottom: (b) FC NSI parameters of $\varepsilon_{e\tau}^{eL}$ and $\varepsilon_{e\tau}^{eR}$ from DS1-CsI(Tl) on $\bar{\nu}_e-e$. The allowed regions from the LSND experiment on ν_e-e are superimposed. The constraints in the $(\varepsilon_{e\mu}^{eL}, \varepsilon_{e\mu}^{eR})$ plane are the same as those of $(\varepsilon_{e\tau}^{eL}, \varepsilon_{e\tau}^{eR})$ in (b).

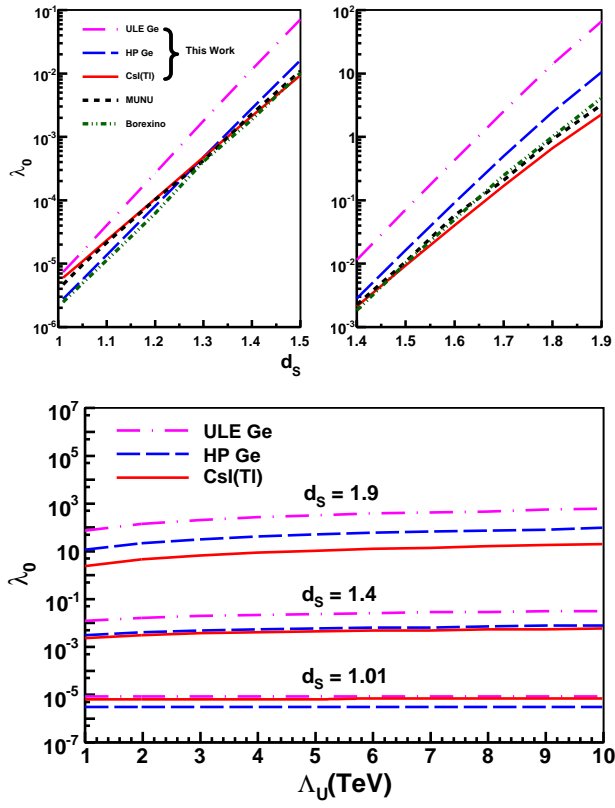


Figure 5: Constraints on UP with scalar exchange – Top: (a) The coupling λ_0 versus mass dimension d_S at $\Lambda_U = 1$ TeV; Bottom: (b) Upper bounds on λ_0 at different energy scales Λ_U . Parameter space above the lines is excluded.

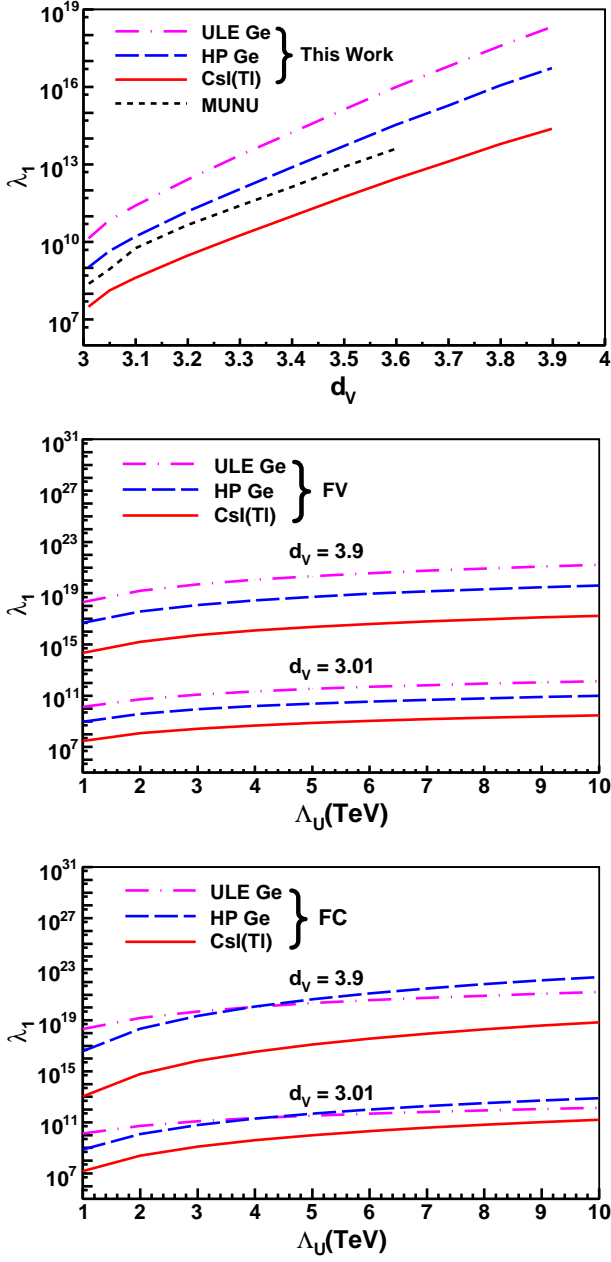


Figure 6: Constraints on UP with vector exchange – Top: (a) The coupling λ_1 versus d_ν at $\Lambda_U = 1$ TeV. The bounds apply for both FV and FC cases. Middle (b) and Bottom (c): Upper bounds on λ_1 at different energy scales Λ_U for FV and FC couplings, respectively, at two values of d_ν . Parameter space above the lines is excluded.